Video System to Monitor Archeological Sites Using Ground-Based Photogrammetry

Article *in* Journal of Surveying Engineering · February 1998

DOI: 10.1061/(ASCE)0733-9453(1998)124:1(3)

CITATIONS
6

READS
74

2 authors:

Mohammed Taleb Obaidat
Jordan University of Science and Technology; Jadara University
99 PUBLICATIONS **376** CITATIONS
SEE PROFILE

H. R Al-Masaeid
Jordan University of Science and Technology
86 PUBLICATIONS **1,139** CITATIONS
SEE PROFILE

VIDEO SYSTEM TO MONITOR ARCHEOLOGICAL SITES USING GROUND-BASED PHOTOGRAMMETRY

By Mohammed Taleb Obaidat[1] and Hashem R. Al-Masaeid,[2] Members, ASCE

ABSTRACT: An attempt was made to investigate the state-of-the-art use of a digital and near real-time system to monitor monuments and historical sites by integrating semiautomated PC-based computer vision and stereo-photogrammetric techniques. The effects of the number and type of control, particularly three-dimensional point location and distance, on the reliability and effectiveness of camera calibration procedures using planar objects as a control facility were studied. The trends of interior and exterior calibration parameters were investigated using 25 combinations of different numbers of measured distances and 3-D control points, and with a fixed focal length for the calibrated charge-coupled device (CCD) cameras. Results showed that increasing the number of distances and 3-D control points above the minimum required control numbers had a slight effect on the values of interior geometry parameters of CCD cameras as well as on the planar object coefficients. The consistency of all test results, except those with control greater than 10 distances and 20 control points, was the major reason for choosing the minimum amount of control for calibration. Quantification of the standard error of image coordinate residuals, distances residuals, standard error of unit weight, and number of iterations for convergence of algorithms supported this result. A historical statue was mapped using single camera operation and a multiple model mapping approach to reconstruct a digital 3-D surface model and thus compute the statue's geometrical characteristics. Three stereo models of the scene were captured from different perspectives. A movable cubic control facility located in the field of view of the mapped scene was used to scale the stereo models. A digital model for the statue was constructed, along with cross sections taken at selected height intervals. The mapping and camera calibration procedures were simple and practical.

INTRODUCTION

Jordan has many important historical and tourist sites spread throughout the country. These historical sites are considered major sources of income and development. Examples of these well-known archeological sites include Petra, Umm-Qais, Jarash, and Ajloun. For restoration and preservation, three-dimensional measurement was required in order to preserve the uniqueness of these monuments. In addition, maintenance requirements and surface deterioration of these monuments require computational procedures to quantify and assess damage to estimate repair needs. Short-term and long-term rates of loss of material due to environmental and human effects must also be monitored (Pillmore et al. 1992; Sherwood 1992). Consequently, the reconstruction of the 3-D object, as well as quantification of by-products such as point locations, areas, and volumes, was required. Stereo-photogrammetry was the most viable and reliable source for extracting useful information because of the availability of unlimited numbers of stereo-pairs for each image. Therefore, actual site inspection is not required after the process of stereo image capture. Instead, computer technology allows office work to be con-

[1]Asst. Prof. of Civ. Engrg., Civ. Engrg. Dept., Jordan Univ. of Sci. and Technol., P.O. Box 3030, Irbid, Jordan.

[2]Assoc. Prof. of Civ. Engrg., Jordan Univ. of Sci. and Technol.

Note. Discussion open until July 1, 1998. To extend the closing date one month, a written request must be filed with the ASCE Manager of Journals. The manuscript for this paper was submitted for review and possible publication on December 5, 1996. This paper is part of the ***Journal of Surveying Engineering***, Vol. 124, No. 1, February, 1998. ©ASCE, ISSN 0733-9453/98/0001-0003–0025/$4.00 + $.25 per page. Paper No. 13715.

ducted in a convenient environment, especially if an automated knowledge-based system is incorporated with stereo photogrammetric metrology (Obaidat and Wong 1996a).

Photogrammetric restitution, which has not been regularly employed in Jordan, has been used for historical monuments with modern analytical stereo-plotting equipment (Abdel-Aziz 1982; Silva and Gomes 1992). The method showed high potential accuracy but does require a specialized photogrammetric operator as well as expensive equipment and time. Other researchers have proposed videocameras and scanners for the same purpose (Ahmed 1981). This system has a major drawback: It does not provide information (i.e., an image) directly to the computer.

This paper investigates the state-of-the-art use of a digital, near real-time, practical ground-based stereo-photogrammetric system to monitor the archeological sites and to perform measurement tasks of other methodologies. Specific objectives include: (1) studying the effect of types and numbers of control points on camera calibration parameters using a planar object facility; and (2) performing a practical procedure for digital 3-D surface mapping of an archeological scene.

PROBLEMS ASSOCIATED WITH COMPUTER VISION

Integration of computer vision technology with stereo-photogrammetry to produce an on-line surface mapping system involves many problematic issues (Wong 1992; Ke 1995), including:

- Warm-up and stability effect of the data acquisition system
- Camera configuration
- Lighting and contrast
- Reliability of camera calibration procedures
- Automatic stereo-image matching and error detection procedures
- 3-D surface reconstruction
- Recognition
- Propagation of image-processing error

This means that full automation of accurate 3-D computation procedures is a long way in the future. Consequently, a near real-time system should be introduced to bridge this gap in technology. This system should have specific requirements, such as an efficient accuracy potential that is compatible with engineering requirements, low-cost hardware, and ease of use.

SYSTEM'S LABORATORY ENVIRONMENT

The proposed system is a PC-based vision system, which was available at the Photogrammetry and Vision Laboratory, Jordan University of Science and Technology (JUST), Jordan. As shown in Fig. 1, the system consists of assembled off-the-shelf, PC-based digital image acquisition components. The use of the system was restricted to image capture (digitization). The main components of the system are:

- An EPIX frame grabber with a 20 MHz pixel clock and 1 MB of image memory (EPIX 1994)
- An interactive Silicon Video Mux software program that digitizes, processes, archives, and displays video images

J. Surv. Eng. 1998.124:3-25.

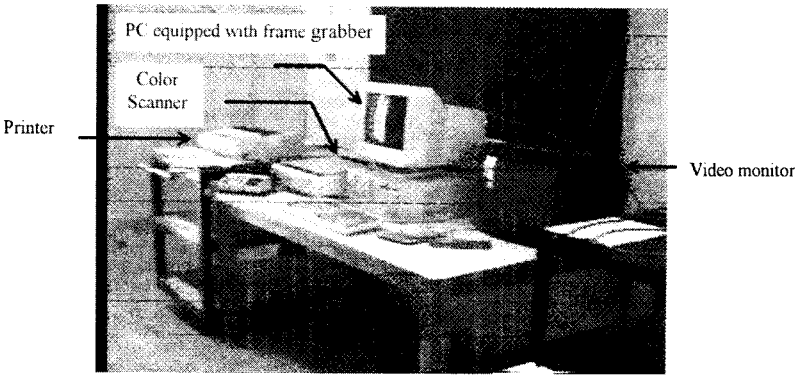

FIG. 1. Off-the-Shelf PC-Based Vision System Components

- A SVGA DTK 486 60 MHz personal computer with 16 MB RAM and a 550 MB hard disk
- A video monitor for image display

The system was supported by two SCX 800 8 mm CCD Samsong camcorders equipped with zoom lens capability. The system has data-exchanging capability within the MS-DOS environment. Due to hardware limitations, video data could be digitized with a maximum spatial resolution of 752(pixels/line)*480(lines/image). Better resolution of about 2,048*2,048 pixels is possible when the frame grabber is upgraded to 4 MB RAM.

CAMERA CALIBRATION SCHEME

To determine the metric characteristics of the camera system for subsequent stereo-photogrammetry field operations, camera calibration was required. This calibration involved correction and modeling of all important factors that affected the image-point positions on the image plane, including the distortion of the bundle of optical rays. It normally involved interior and exterior orientation parameters. The interior orientation defines the form of the bundle of rays passing from the object point through exposure center to the image plane. Interior orientation parameters include: symmetrical radial distortion parameters (l_1, l_2, and l_3), decentering radial distortion parameters (p_1, p_2, and P_3), principal point (x_p, y_p), focal length (f), and affine scale (k). The exterior orientation parameters include the position of the exposure center (X^c, Y^c, and Z^c) and orientation of the optical axis (ω, ϕ, and κ) of the camera in the object-space. The mathematical model used to calibrate individual images can also be found elsewhere (Wiley 1991).

Properly Oriented Cameras

Using two cameras properly oriented with respect to each other in stationary positions for the purpose of stereo measurement involves the determination of both interior and exterior orientation parameters (i.e., the relative positions of the cameras with respect to each other). This process should be completed before mounting the two cameras for use at a proposed measurement site. A 3-D laboratory control field or planar wall facility could be used for the calibration process (Karara 1989; Wiley 1991; Obaidat and Wong

1996b). Dual cameras should be distributed in the archeological site such that their fields of view cover the whole scene.

Single Camera Operation

Single cameras should be calibrated for interior geometry only, while a movable control field was used for scaling purposes. An efficient method for identifying the interior calibration parameters for the CCD cameras was the use of a planar object, such as a brick wall, which is available almost everywhere. Fig. 2 shows an example of the used planar wall facility. Mortar joints were used as image targets. At least three control points of known coordinates must be available in the mapped scene to perform model scaling with respect to the ground coordinate system. For practicality, a movable object of control could be used. Fig. 3 is a 3-D drawing of a cube used as a control facility in this research. The target point locations at the corners of adjacent square

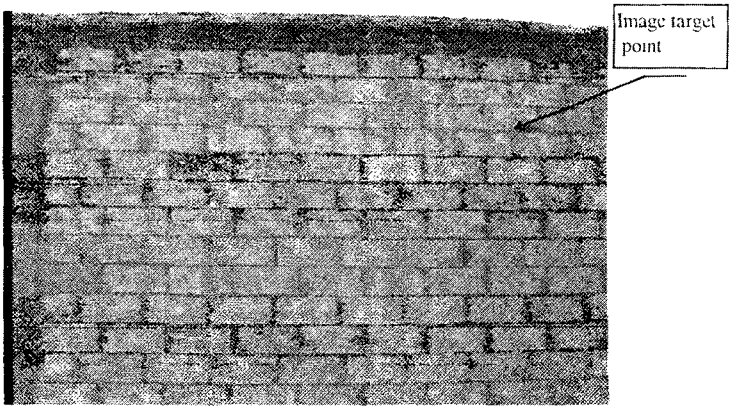

FIG. 2. Planar Wall Calibration Facility

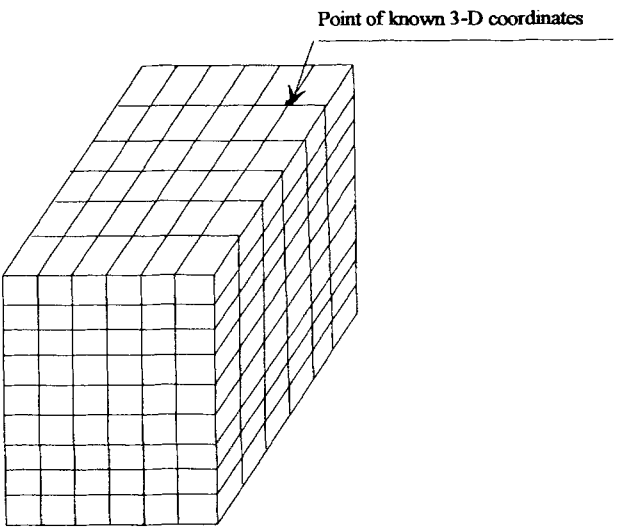

FIG. 3. 3-D Movable Cubic Control Facility

meshes were surveyed to 1 mm accuracy. The dimensions of the grid (10 cm × 10 cm) are dependent on camera resolution as well as object distance, which permitted definition of square corners in the digital image. The cube has to be located in the common area of each stereo pair.

Condition Equations of Planar Object Control

Enforcing the conjugate bundle of rays to intersect on a planar (flat) object involves: (1) n plane observation equations for n target points appearing on the stereo image; (2) m control distance observation equations; and (3) 15 observation equations for unknows (including interior and exterior orientation parameters of the two camera locations). The least-squares model to solve for corrections of unknown parameters can be written in the following matrix form (Obaidat and Wong 1996b):

$$\begin{bmatrix} \dot{\mathbf{A}}_{(n,4n)} & 0 & 0 \\ 0 & \ddot{\mathbf{A}}_{(m,m)} & 0 \\ 0 & 0 & \mathbf{I}_{(15,15)} \end{bmatrix} \begin{bmatrix} \dot{\mathbf{V}}_{(4n,1)} \\ \ddot{\mathbf{V}}_{(m,1)} \\ \dddot{\mathbf{V}}_{(15,1)} \end{bmatrix} + \begin{bmatrix} \dot{\mathbf{B}}_{(n,15)} \\ \ddot{\mathbf{B}}_{(m,15)} \\ -\mathbf{I}_{(15,15)} \end{bmatrix} \dot{\Delta}_{(15,1)} = \begin{bmatrix} \dot{\boldsymbol{\varepsilon}}_{(n,1)} \\ \ddot{\boldsymbol{\varepsilon}}_{(m,1)} \\ \dddot{\boldsymbol{\varepsilon}}_{(15,1)} \end{bmatrix} \quad (1)$$

where $\dot{\mathbf{A}}$, $\ddot{\mathbf{A}}$ = residual coefficient matrices for stereo image points and measured distances, respectively; $\dot{\mathbf{V}}$, $\ddot{\mathbf{V}}$, $\dddot{\mathbf{V}}$ = residual matrices for stereo image points, measured distances, and unknown parameters, respectively; $\dot{\mathbf{B}}$, $\ddot{\mathbf{B}}$ = coefficient matrices for stereo image points and measured distances, respectively; $\dot{\boldsymbol{\varepsilon}}$, $\ddot{\boldsymbol{\varepsilon}}$, $\dddot{\boldsymbol{\varepsilon}}$ = discrepancy matrices for stereo image points, measured distances, and unknown parameters, respectively; $\mathbf{I}$ = identity matrix; $\dot{\Delta}$ = vector of corrections for unknown parameters; n = number of given stereo image points; and m = measured distances.

Fifteen corrections of the unknowns were continually added to their approximated values after each iteration until the convergence criterion was reached. Consequently, the 15 unknown values representing the interior and exterior orientations of the camera could be quantified. These unknowns include:

- Planar facility parameters (A, B, and C)—i.e., the coefficients of the plane equation in which the plane intersects the object-space coordinate system (X, Y, and Z)
- Right camera exterior orientation parameters (X_r^c)—i.e., x-axis exposure center coordinate of the right camera position
- Three rotation parameters around the three axes of the right camera position (ω_r, φ_r, κ_r)
- Principal point coordinates (x_p, y_p)
- Radial lens distortion parameters (l_1, l_2)
- Decentering distortion parameters (P_1, P_2, and P_3)
- Affine scaling parameter (k)

SURFACE MEASUREMENTS

Fig. 4 shows the sequence of procedures developed in this research work to quantify object-space surface measurements. It starts with three types of input: stereo image points digitization, weighted least-squares camera calibration procedure, and control identification. Then, stereo image matching of corresponding image targets was implemented using a pyramidal matching (Lew 1990). This is an interactive matcher program that yields subpixel accuracy using different window sizes, convergence criteria, and a maximum

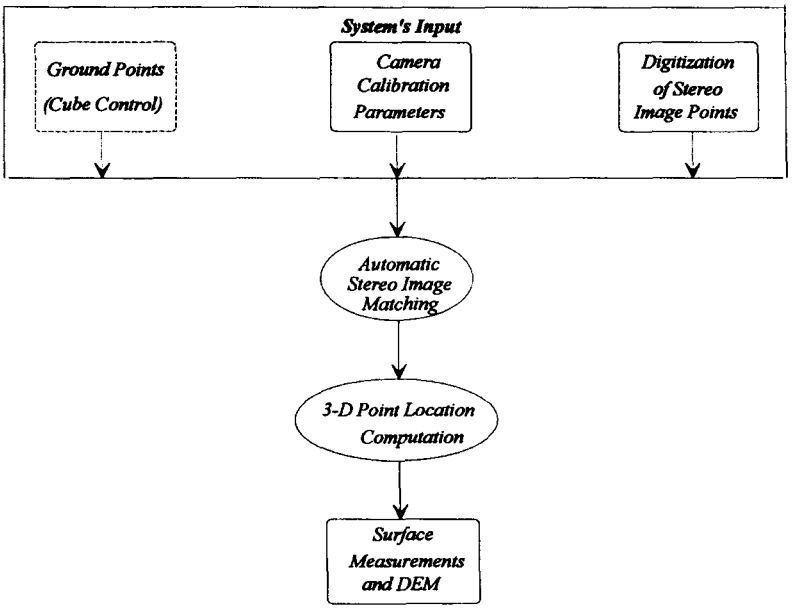

FIG. 4. Sequence of Procedures to Quantify Object-Space Surface Measurements

number of iterations. It also has different matching criteria based on intensity, threshold, and x and y gradients. Object-space coordinates are found by applying a space intersection algorithm (Wong 1980). By-product values, such as distances, perimeters, surface areas, and volumes, can be found using a cross-section-based algorithm. The algorithm projects closed contours cross sections of equal height object-space intervals. Consequently, all by-product parameters can be computed from one contour, but volume is computed from two adjacent contours. A digital elevation model (DEM) can also be produced (Obaidat et al. 1997).

When a movable camera is used for site operations, relative and absolute orientation procedures have to be performed with the aid of the cube control facility.

During use of stationary precalibrated dual cameras, when object points are moved from their places the system sounds an alarm to alert the human operator that theft or damage has occurred. Therefore, the monitoring of archeological sites, or any scene, could be controlled in a semi-automatic and near real-time manner. The monitoring process used in this approach has the potential of providing 3-D visualization as well as 3-D coordinate for quantification of the scene, unlike the surveillance cameras, which provide only a 2-D scene.

Multiple Models

Because of the difficulties associated with mapping entire objects in a single stereo model, a series of overlapped stereo views from different positions were required to overcome problems of occlusion. In addition, large-scale images have to be captured to overcome the limitation of a small field of view and low resolution of the CCD cameras to meet the accuracy require-

ments. Camera and image configuration normally guides this process. Control features (joints)—not surveyed points—have to be identified in the scene to join the separate stereo pairs and consequently to find 3-D ground points. Three-dimensional control points were required when using single camera operation, while identification of the control points was needed only for scaling and translation of a stereo model in the case of properly oriented dual cameras.

GROUND POINTS AND DISTANCE CONTROLS

Accurate quantification of camera calibration parameters is the key to accurate surface measurement extraction. Consequently, it was worthwhile to study the effect of the number and type of controls on the reliability and effectiveness of camera calibration procedures. This study was performed by calibrating two CCD cameras using a planar wall facility that had over 200 target points. The planar wall calibration procedure has the advantage of intersecting all conjugate pairs of rays at points located on a constrained plane (Obaidat and Wong 1996b). The planar wall calibration procedure was performed using different combinations of 3-D ground control points and a number of measured distances. The two control types, including 3-D ground points and distances, were located on the planar wall. The following numbers of 3-D control points were used: 4, 6, 9, 15, and 20. The numbers of control distances used were 4, 6, 8, 10, and 15. These numbers were minimized to make the calibration procedure simple and practical.

The software package CCDCAL_PLANE was used to calibrate the CCD cameras using the single camera operation procedure (Obaidat and Wong 1996b). The two CCD cameras to be calibrated had the same trademark and specifications and therefore approximately the same interior geometry. The cameras were mounted on a stand prepared specifically for this study. The base of the stereo images was about 80 cm, which was the maximum possible separation between the two locations of the cameras using this stand. A focal length of about 11 mm (equivalent to about 1,034 pixels) was selected for this study, with an object distance to the planar wall of about 5.5 m, to achieve comparable resolution and accuracy. Other precautions, such as warming up the cameras and controlling environmental temperature and humidity, were taken. A sizable number of possible combinations of distances and 3-D ground points control were studied: 25 cases of control combinations of 3-D points and distances.

Figs. 5–7 show the effect of different control combinations of 3-D points and measured distances on: principal point coordinates (x_p, y_p) and affine scaling parameter (k); radial and decentering distortion parameters (L_1, L_2, P_1, P_2, and P_3); and planar wall coefficients (A, B, and C). Fig. 5 shows a slight change in principal point coordinates resulting from changes in the numbers of 3-D and distance controls. The change in principal point coordinates with changing the number of 3-D and distance controls was consistently less than 20 pixels for all tested combinations except those with 10 distances and 15 control points (for which it was 40 pixels). The results were consistent for all the computed principal point coordinates, except those with 10 distances and 15 control points. This was the reason for using the minimum control case of four 3-D control points and four measured distances on the planar wall to calibrate the CCD camera. The affine scaling parameter had similar trend of a change consistently less than 1.0×10^{-2}. A similar trend of results was obtained for the radial and decentering distortion parameters, shown in Fig. 6. Because of the consistency of the radial and de-

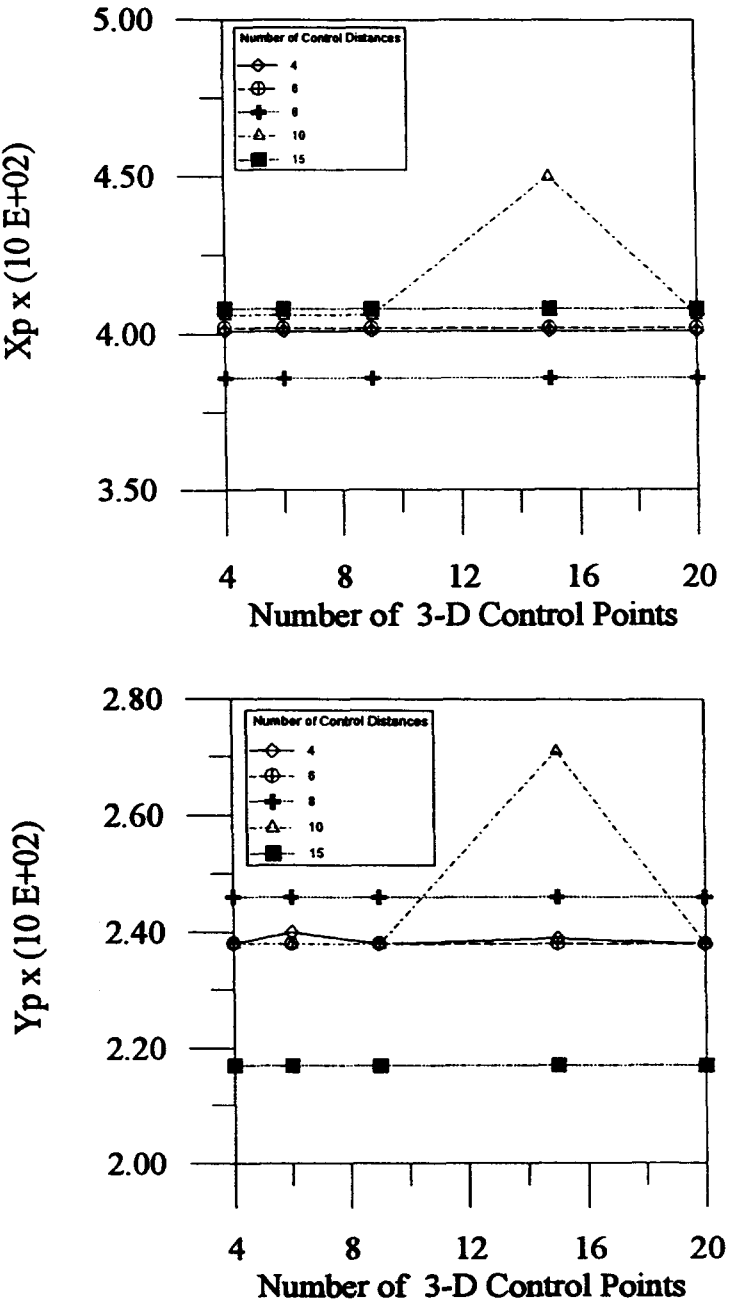

FIG. 5. Effect of Combinations of Different 3-D Control Points with Variable Numbers of Measured Control Distances on Principal Point Coordinates (in Pixels) and Affine Scaling Parameter

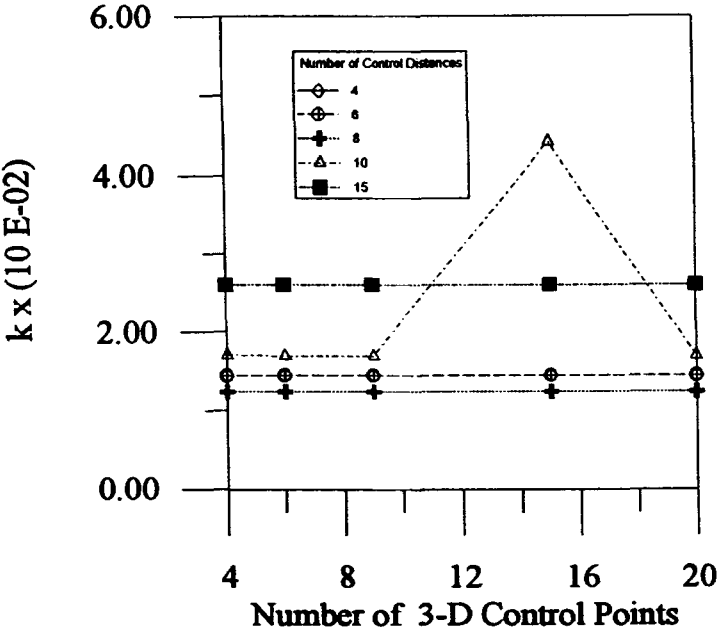

FIG. 5. (*Continued*)

centering distortion parameters in all tests (except those with 10 distances and 15 control points), only the minimum control case of four 3-D control points and four measured distances was used to calibrate the CCD camera. The value of any single calibration parameter does not give any indication of the accuracy of the calibration procedures, but the collective use of all calibration parameters in the calibration model does. Differences in distortion parameters for all combinations reached maximum values of about 3×10^{-7}, 3×10^{-12}, 5×10^{-5}, 2.5×10^{-5}, and 6×10^{-6} pixels, respectively, for L_1, L_2, P_1, P_2, and P_3.

The test case with 10 distances and 15 control points yielded camera calibration results that were inconsistent with other cases. This may be attributed to an error in the data set. Therefore, although the results of the case are reported here, they may be eliminated from consideration.

Figs. 5 and 6 show that changing the number of control distances did seem to affect the calibration results, whereas changing the number of control points appeared to have little effect. This indicates that the minimum number of control points should be used. However, statistical tests—the T test and the chi-square test—showed that the changes in the camera calibration results for different control distances are insignificant. This could lead to the conclusion that changing the number of control distances and control points did affect the calibration results.

Fig. 7 shows the values of the coefficients A, B, and C of the plane equation where the plane intersects the object-space coordinate system (X, Y, and Z). The control combinations did not affect 3-D points and distances on the B coefficient because the y-axis coordinates were constant (i.e., the calibration facility was planar). Minor effects were found on coefficients A and C, where the variations due to control combinations do not exceed 2×10^{-13}. The

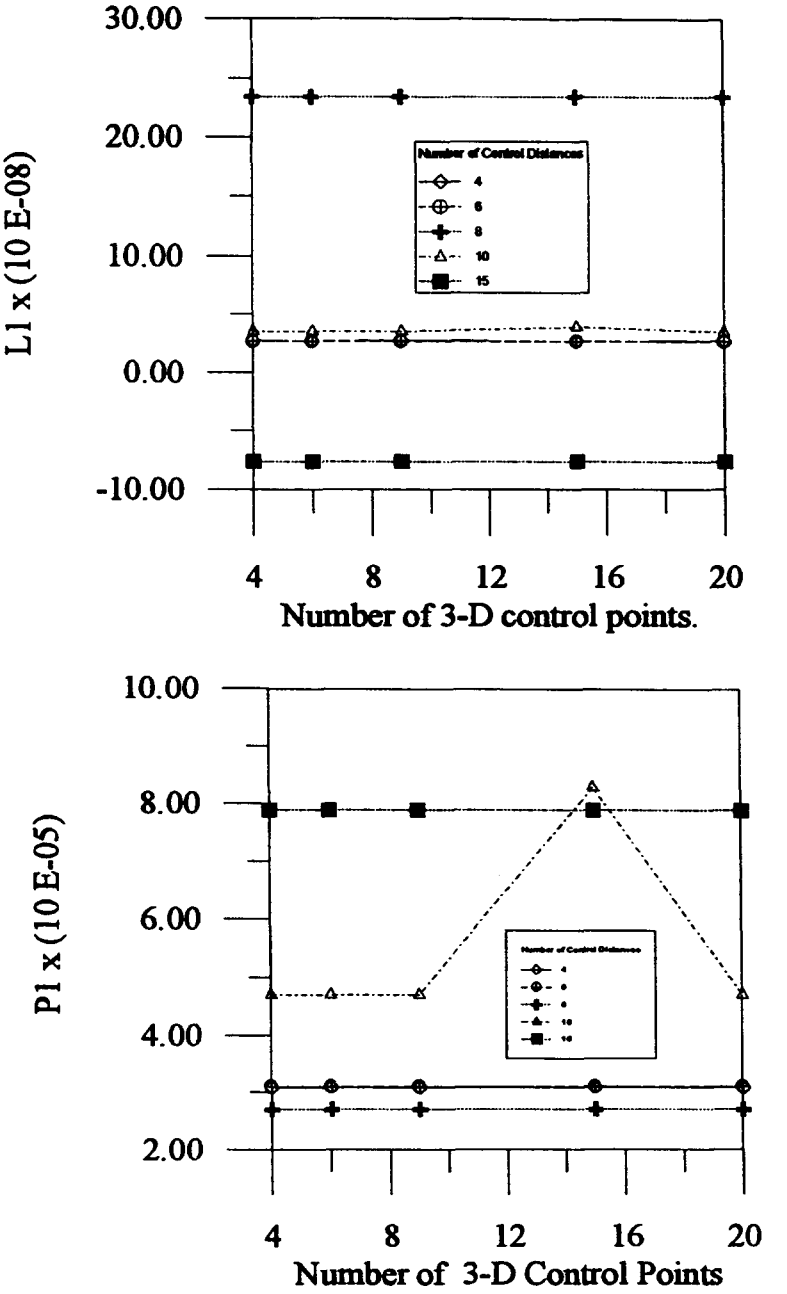

FIG. 6. Effect of Combinations of Different 3-D Control Points with Variable Number of Measured Control Distances on Radial and Decentering Distortion Parameters (in Pixels)

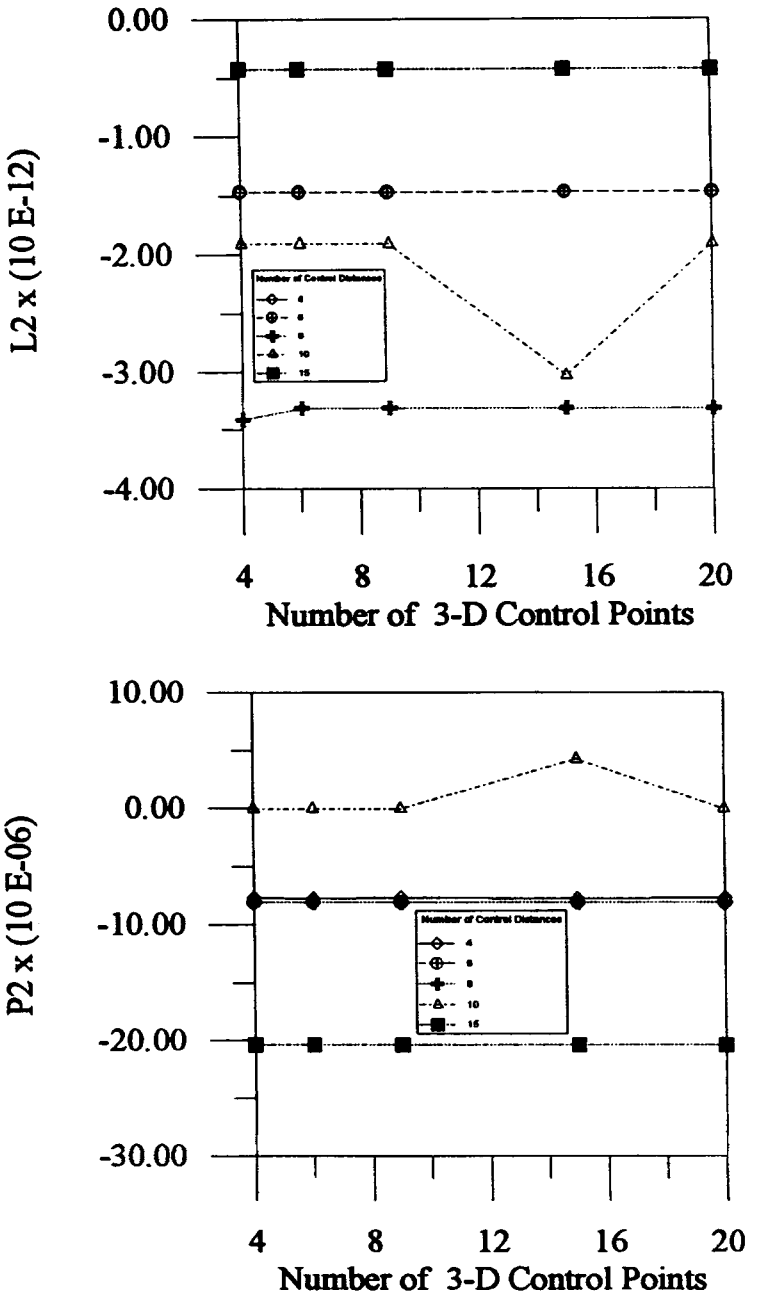

FIG. 6. (*Continued*)

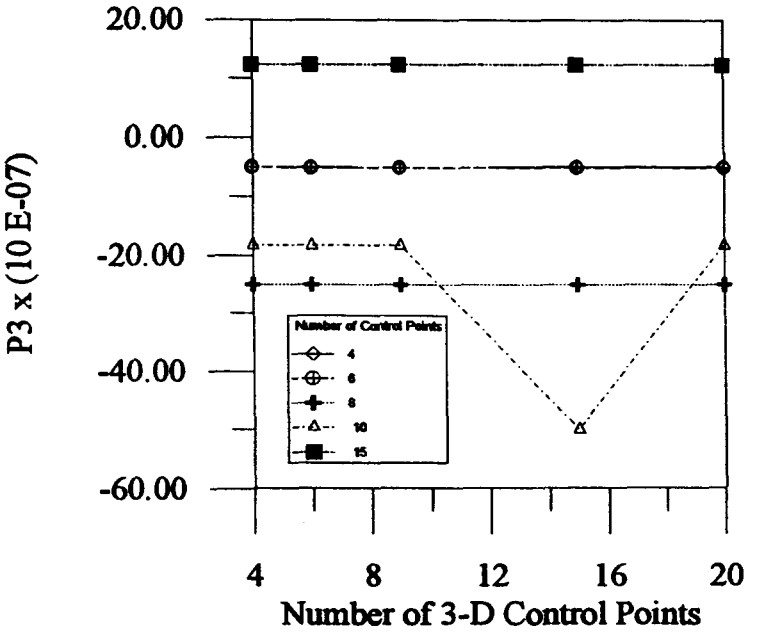

FIG. 6. (*Continued*)

variations may be contributed to the unflatness of and waves on the planar wall.

In conclusion, the combinations of control types using different numbers of 3-D points and measured distances had a slight effect on the values of interior geometry of CCD cameras as well as the planar object coefficients. This means that using the minimum number of controls was quite sufficient. (In fact, this is one of the major advantages of using planar wall calibration procedures.) This result is compatible with previous research, which showed stability of calibration parameters after using certain numbers of stereo image points (Obaidat and Wong 1996b). This result is not similar to the 3-D laboratory calibration procedures, which showed consistent stability of calibration parameters and accuracy of computed surface measurement as the number of surveyed 3-D control field points was increased (Fryer 1989; Wiley and Wong 1992). This may be attributed to: (1) accurately surveyed control points in case of 3-D laboratory calibration; and (2) unflatness of and waves on the planar wall, which affected the consistency of accuracy of the approximated 3-D control points used on the wall.

Residual Errors

Standard deviations and means of computed residual errors of image coordinates as well as control distances, standard errors of unit weight, and number of iterations were normally used to check the effectiveness and performance of calibration procedures. Table 1 and Fig. 8 show these quantities for the 25 control cases used in this study. In case 1 to case 20, standard errors of unit weight were almost constant with changes in the numbers of 3-D control points and distances. The standard error of unit weight (σ_0) was used as a measure of satisfaction for calibration procedures. In cases 21 to

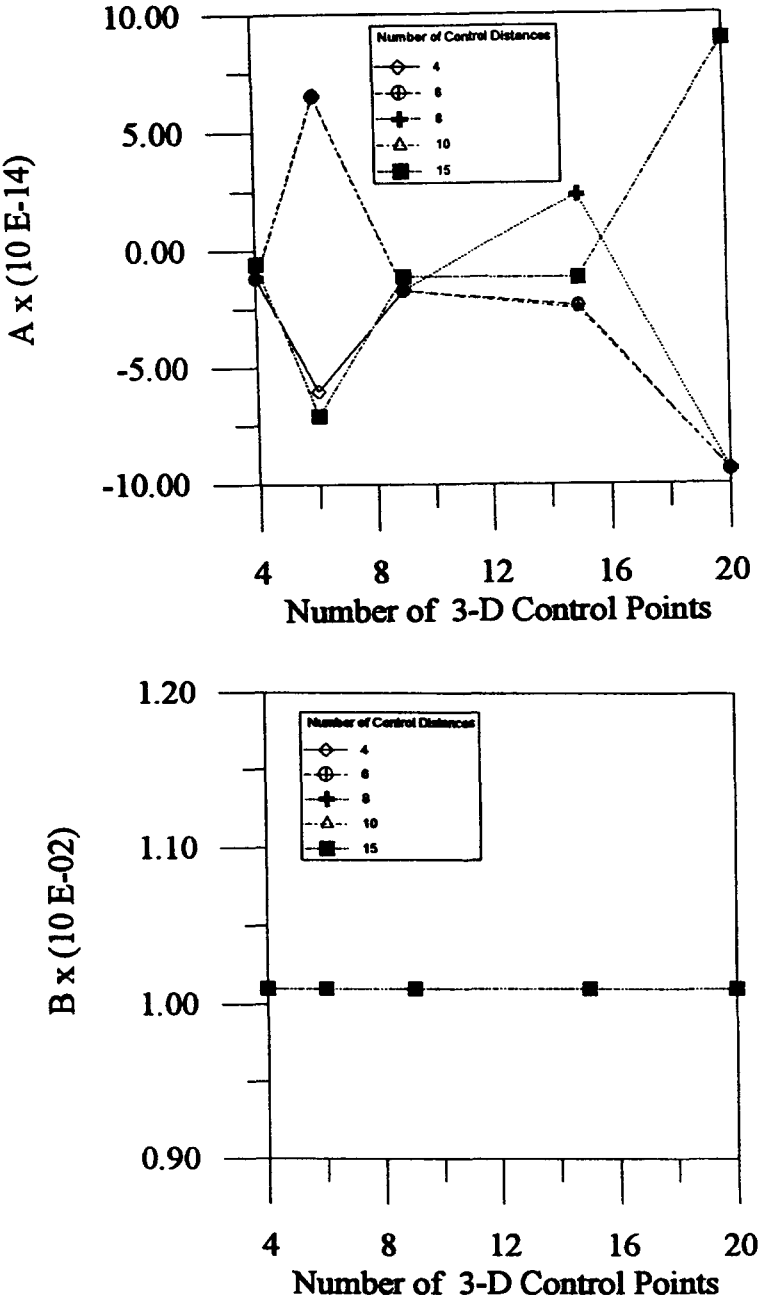

FIG. 7. Effect of Combinations of Different 3-D Control Points with Variable Number of Measured Control Distances on Planar Wall Coefficients

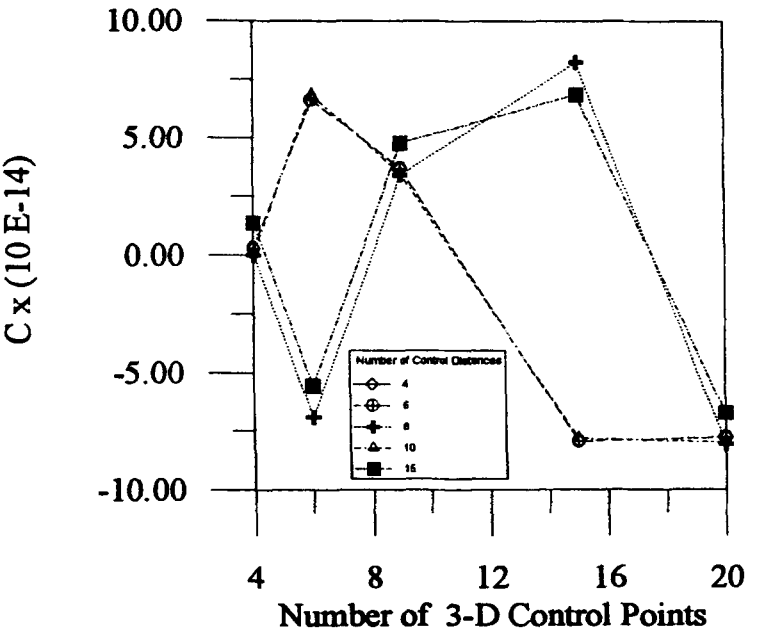

FIG. 7. (*Continued*)

25—i.e., when more than 10 measured distances were used—σ_0 jumped from about 0.9 pixel to about 1.3 pixels for the left camera and from about 0.7 pixel to about 1.7 pixels for the right camera. The standard error of unit weight ranged from about 0.7 to 1.7 pixels for both cameras using an input standard unit weight of unity.

After application of the camera calibration mathematical model, deviations in σ_0^2 were examined for errors and it was found that none existed. The output results of σ_0 were divided into two data sets: (1) data set A for the output of cases 1 to 20; and (2) data set B for the output of cases 21 to 25. For example, σ_0 uncertainty interval for data set A at one standard deviation for the left camera was 0.87 $\pm$ 0.03 pixel and 1.33 $\pm$ 0.0003 pixels for data set B. For the right camera it was 0.75 $\pm$ 0.05 pixel for data set A and 1.67 $\pm$ 0.003 pixels for data set B.

Statistical chi-square tests were carried out to determine the significance of the deviations in the two sets of σ_0 results for each camera. Data set A had 19 degrees of freedom, and B had 4 degrees of freedom. The statistical test indicated that there is a significant difference between the two sets of data at the 99% probability level. T-tests were also conducted to examine the difference of results between the means of the two sets. Similarly, these test results indicated that the difference between the means was significant at the 99% probability level. Therefore, results associated with data set B—the results of cases 21 to 25—should be excluded from the analysis, and conclusions should be based on the consistent results of cases 1 to 20. The consistency of the test results in data set A is the major reason for choosing the minimum number of controls for calibration.

The standard errors of residuals of image coordinates showed a similar trend. The standard errors in the x-axis of image coordinates (σ_x) for both

cameras ranged from 0.5 to 0.8 pixel. The standard error in the y-axis of image coordinates (σ_y) ranged from 0.05 to 0.08 pixel because of the planar wall constraint in the y-axis. The resultant vector of xy standard error of residuals (σ_{xy}), also followed the same trend of change as the standard error of unit weight. In cases 1 to 20, it was almost constant at 0.4 and 0.3, respectively, for left and right cameras. Then, a sudden jump in its value to about 0.5 pixel occurred for both cameras. This supports the previously mentioned conclusion that the consistency of the test results, except those associated with cases 21 to 25, suggest that the minimum number of controls for calibration should be used. This means that no accuracy problems will affect camera calibration parameters when using the minimum number of controls. The mean of residuals of image coordinates was about zero pixel because of the random selection of stereo image points.

The computed residuals of distances showed a trend similar to those previously mentioned for σ_0 and σ_{xy}. The number of iterations, which was a measure of computing time efficiency of the calibration procedures, followed exactly the same trend. Consequently, using the minimum control case with any combination of 3-D control leads to a consistent minimization of σ_0, σ_{xy}, and distances residuals and decreases running time for computational procedures of calibration parameters. This was due to difficulties of convergence for the calibration mathematical model when the number of observations were increased. Increasing the number of measured control points and distances created the problem of discontinuity in the results in cases 21–25.

MAPPING OF HISTORICAL STATUE

A historical statue in the city of Umm-Qais (Gadara), located in the north part of Jordan, was mapped using the multiple model approach described previously. The statue was mapped for the purpose of building a digital 3-D surface model to compute its geometrical characteristics. Single camera operation was used in this study, with a fixed focal length of 11 mm. A planar wall facility was used to define the interior geometry of the camera. A movable cubic control field in the field of view of the mapped scene was used to scale the stereo models.

Fig. 9 shows a pair of stereo images of the statue captured from one perspective. An object distance of about 6.0 m and camera base of about 2.0 m were used. Therefore, one pixel in the image domain was equivalent to about 6 mm in object-space coordinates (1 pixel in image domain $\approx$ 0.02 μm). Because of its relatively small size, the statue fit within the camera's field of view. This was a great advantage when making geometric measurements of each side of the statue using a single camera setup. Since the texture and topography of the statue surface had intensity variations, there was no need to project target points on or attach target points to the statue. Stereo image points for each stereo model were digitized for all possible edge points on the statue. Over 300 target points were used for the three stereo models. A minimum of three tie points on the statue were used to integrate three stereo models from different locations with different orientations. The object-space coordinates from the three stereo model perspectives were merged by using 3-D coordinate transformation procedures—the absolute orientation process. This process unified the reference of the three ground coordinate systems.

The computed 3-D coordinates was used for digital surface mapping. Fig. 10 shows a digital surface model of the mapped statue made using surface measurement procedures. This model shows the 3-D view of the object as well as cross sections generated at any selected vertical interval of the object.

TABLE 1. Residual Errors of Image Coordinates as well as Control Distances, Standard Errors of Unit Weight, and Number of Iterations

Case number (1)	Number of measured distances (2)	Number of control XYZ points (3)	σ_0 (4)	σ_x (5)	σ_y (6)	σ_{xy} (7)	Mean (8)	Distances residuals (9)	Ratio of final σ_0 to given σ_0 (10)	Number of iterations (11)
					(*a*) Left Camera					
1	4	4	8.492E-01	5.536E-01	4.822E-02	3.816E-01	2.298E-04	2.376E-03	8.499E-01	7
2	4	6	8.493E-01	5.536E-01	4.825E-02	3.815E-01	2.288E-04	2.379E-03	8.493E-01	7
3	4	9	8.492E-01	5.538E-01	4.822E-02	3.815E-01	2.287E-04	2.375E-03	8.492E-01	7
4	4	15	8.493E-01	5.356E-01	4.825E-02	3.815E-01	2.293E-04	2.379E-03	8.493E-01	7
5	4	20	8.493E-01	5.536E-01	4.822E-02	3.186E-01	2.300E-04	2.375E-03	8.493E-01	7
6	6	4	8.346E-01	5.537E-01	4.826E-02	3.815E-01	1.299E-04	1.829E-03	8.346E-01	7
7	6	6	8.346E-01	5.537E-01	4.826E-02	3.815E-01	1.303E-04	1.829E-03	8.346E-01	7
8	6	9	8.346E-01	5.537E-01	4.826E-02	3.815E-01	1.303E-04	1.829E-03	8.346E-01	7
9	6	15	8.346E-01	5.537E-01	4.826E-02	3.815E-01	1.312E-04	1.829E-03	8.346E-01	7
10	6	20	8.346E-01	5.537E-01	4.826E-02	3.815E-01	1.298E-04	1.829E-03	8.346E-01	7
11	8	4	8.943E-01	5.676E-01	4.994E-02	3.812E-01	−7.943E-04	5.585E-03	8.943E-01	8
12	8	6	8.943E-01	5.676E-01	4.994E-02	3.812E-01	−7.943E-04	5.585E-03	8.943E-01	8
13	8	9	8.943E-01	5.676E-01	4.994E-02	3.812E-01	−7.943E-04	5.585E-03	8.943E-01	8
14	8	15	8.943E-01	5.676E-01	4.994E-02	3.812E-01	−7.943E-04	5.585E-03	8.943E-01	8
15	8	20	8.943E-01	5.676E-01	4.994E-02	3.812E-01	−7.943E-04	5.585E-03	8.943E-01	8
16	10	4	9.121E-01	5.583E-01	4.999E-02	3.960E-01	4.033E-04	3.811E-03	9.121E-01	7
17	10	6	9.121E-01	5.583E-01	4.999E-02	3.960E-01	4.036E-04	3.811E-03	9.121E-01	7
18	10	9	9.122E-01	5.826E-01	4.999E-02	3.960E-01	4.036E-04	3.811E-03	9.122E-01	7
19	10	15	9.287E-01	5.632E-01	5.256E-02	2.918E-01	−1.056E-04	4.461E-03	9.287E-01	19
20	10	20	9.121E-01	5.526E-01	4.999E-02	3.960E-01	4.035E-04	3.811E-03	9.121E-01	7
21	15	4	1.326E 00	6.737E-01	5.463E-02	4.486E-01	−4.770E-04	8.940E-03	1.326E 00	11
22	15	6	1.326E 00	6.737E-01	5.463E-02	4.486E-01	−4.773E-04	8.941E-03	1.326E 00	11

23	15	9	1.326E 00	6.737E-01	5.463E-02	4.486E-01	−4.774E-04	8.941E-03	1.326E 00	11
24	15	15	1.326E 00	6.737E-01	5.463E-02	4.486E-01	−4.776E-04	8.941E-03	1.326E 00	11
25	15	20	1.326E 00	6.737E-01	5.463E-02	4.486E-01	−4.776E-04	8.941E-03	1.326E 00	11
					(*b*) Right Camera					
1	4	4	7.555E-01	4.622E-01	3.796E-02	2.787E-01	1.220E-03	8.066E-03	7.555E-01	7
2	4	6	7.555E-01	4.622E-01	3.797E-02	2.787E-01	1.220E-03	8.066E-03	7.555E-01	7
3	4	9	7.555E-01	4.622E-01	3.796E-02	2.786E-01	1.220E-03	8.066E-03	7.555E-01	7
4	4	15	7.555E-01	4.622E-01	3.796E-02	2.786E-01	1.220E-03	8.066E-03	7.555E-01	7
5	4	20	7.555E-01	4.622E-01	3.796E-02	2.786E-01	1.220E-03	8.066E-03	7.555E-01	7
6	6	4	7.409E-01	4.603E-01	3.889E-02	2.865E-01	1.054E-04	6.859E-03	7.409E-01	14
7	6	6	7.409E-01	4.603E-01	3.889E-02	2.865E-01	1.069E-02	6.859E-03	7.409E-01	14
8	6	9	7.409E-01	4.603E-01	3.889E-02	2.865E-01	1.060E-04	6.858E-03	7.409E-01	14
9	6	15	7.409E-01	4.603E-01	3.889E-02	2.865E-01	1.055E-04	6.858E-03	7.409E-01	14
10	6	20	7.409E-01	4.603E-01	3.889E-02	2.865E-01	1.055E-04	6.858E-03	7.409E-01	14
11	8	4	7.237E-01	4.646E-01	3.907E-02	3.023E-01	−5.783E-05	5.489E-03	7.237E-01	10
12	8	6	7.237E-01	4.646E-01	3.907E-02	3.023E-01	−5.776E-05	5.489E-03	7.237E-01	10
13	8	9	7.237E-01	4.634E-01	3.907E-02	3.023E-01	−5.77E-05	5.489E-03	7.237E-01	10
14	8	15	7.236E-01	4.646E-01	3.907E-02	3.023E-01	−5.77E-05	5.489E-03	7.236E-01	10
15	8	20	7.236E-01	4.646E-01	3.907E-02	3.023E-01	−5.77E-05	5.489E-03	7.236E-01	10
16	10	4	9.286E-01	5.632E-01	5.255E-02	2.918E-01	−1.057E-03	4.462E-03	9.286E-01	19
17	10	6	9.287E-01	5.631E-01	5.255E-02	2.918E-01	−1.056E-03	4.461E-03	9.287E-01	19
18	10	9	7.373E-01	4.493E-01	3.944E-02	2.851E-01	−1.041E-03	5.669E-03	7.373E-01	6
19	10	15	7.373E-01	4.493E-01	3.944E-02	2.850E-01	−1.041E-03	5.669E-03	7.373E-01	6
20	10	20	7.373E-01	4.493E-01	3.944E-02	2.850E-01	−1.041E-03	5.669E-03	7.373E-01	6
21	15	4	1.670E 00	7.759E-01	8.035E-02	4.860E-01	−1.047E-03	1.425E-02	1.670E 00	27
22	15	6	1.670E 00	7.770E-01	8.048E-02	4.860E-01	−1.057E-03	1.426E-02	1.670E 00	28
23	15	9	1.670E 00	7.759E-01	8.034E-02	4.860E-01	−1.047E-03	1.425E-02	1.670E 00	27
24	15	15	1.676E 00	7.770E-01	8.048E-02	4.860E-01	−1.057E-03	1.425E-02	1.676E 00	28
25	15	20	1.675E 00	7.759E-01	8.030E-02	4.860E-01	−1.047E-03	1.425E-02	1.675E 00	27

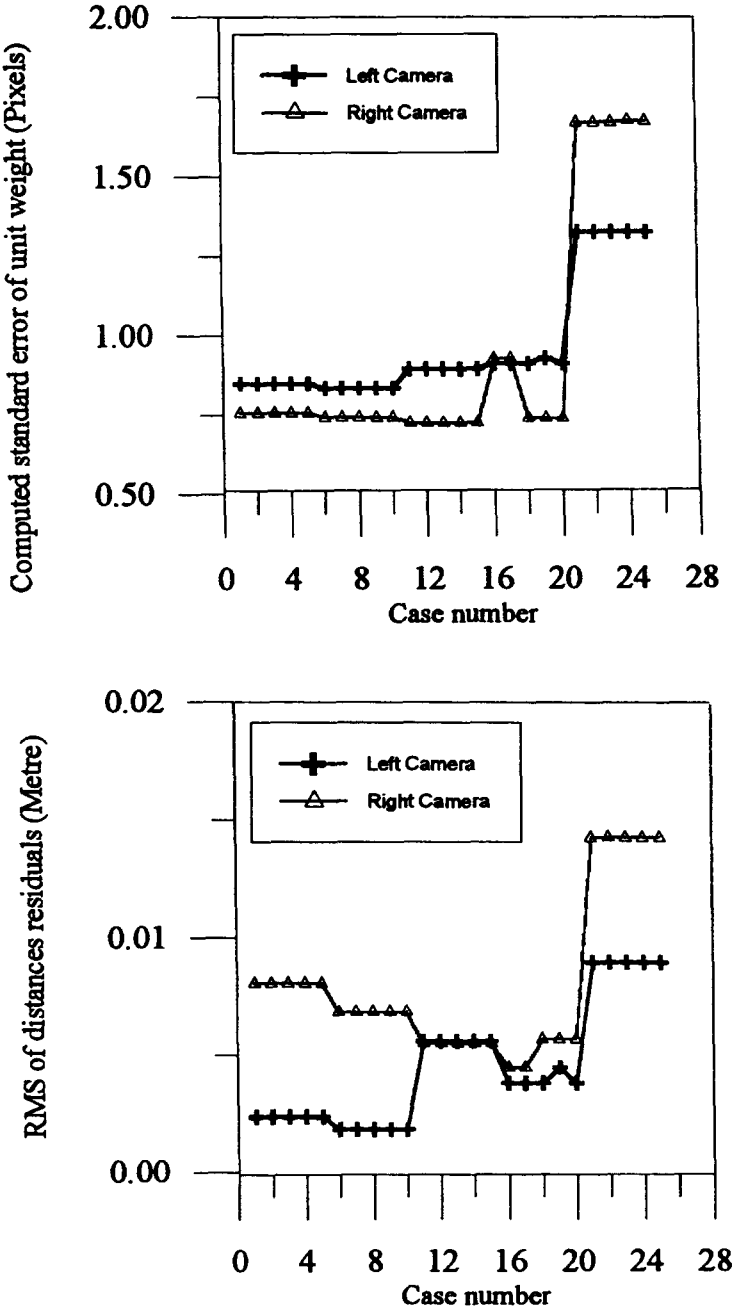

FIG. 8. Standard Deviations and Means of Computed Residual Errors of Image Coordinates (in Pixels) as well as Control Distances (in Meters), Standard Errors of Unit Weight (in Pixels), and Number of Iterations

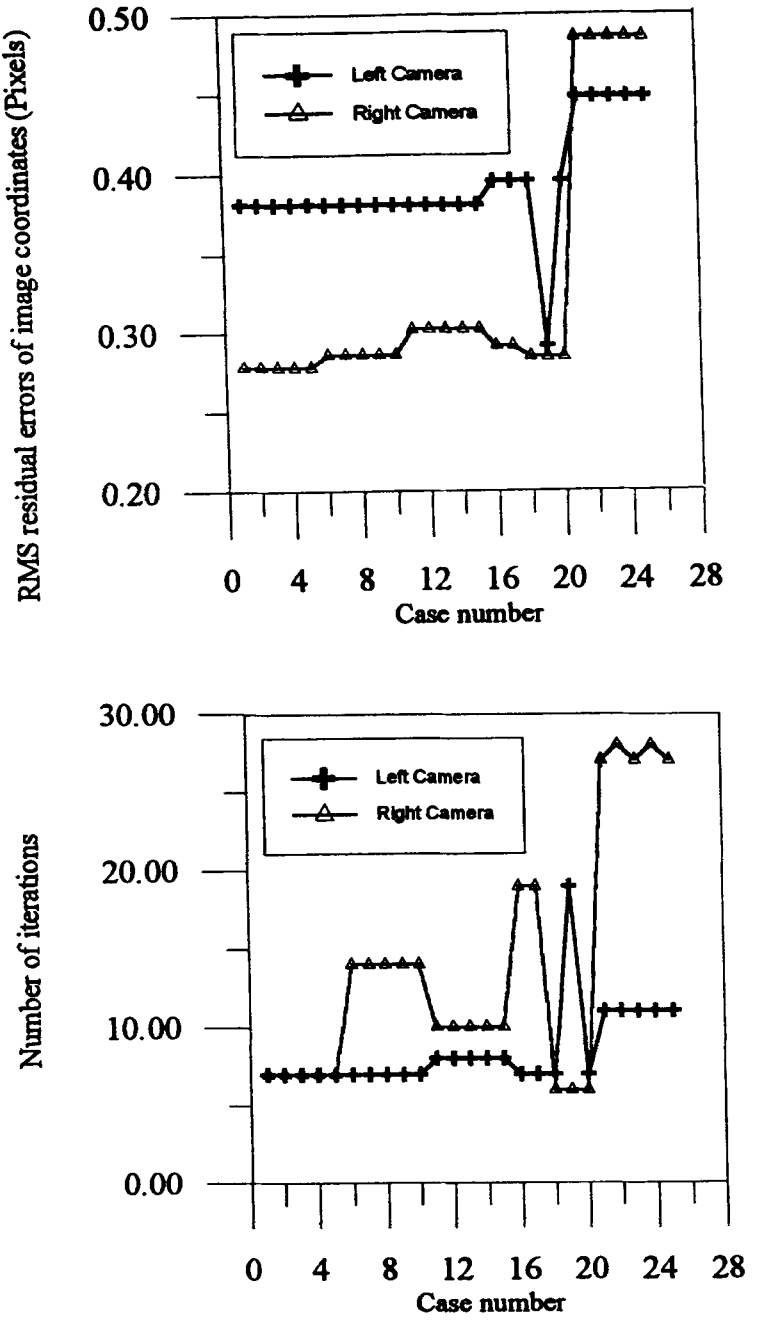

FIG. 8. (*Continued*)

FIG. 9. Stereo Images of Mapped Statue

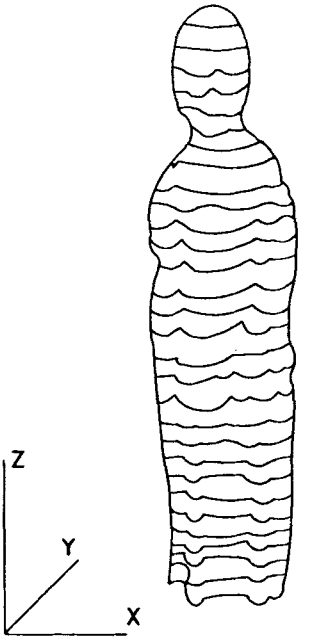

FIG. 10. Digital Surface Model for Mapped Statue

Views of the statue from different perspectives could also be generated. In this particular example, a vertical interval of 5 cm was used for cross section generation. No attempt was made to check the surface measurement accuracy of the statue.

Neither a special lighting facility nor field survey points in the mapped scene was required for image contrast. This procedure could be used in sunlight with single exposures taken from a camera mounted on the shoulder of a human operator, making the developed procedure simple and practical.

Results showed high potential accuracy of the extracted surface measurements using the video system. Ground point coordinates were reported to ± 1 pixel on the image domain. To evaluate the accuracy of the results, volume and surface area were measured using both a conventional procedure (an actual survey) and the vision system. When the 3-D coordinates of the sur-

veyed points on the statue were used, the actual computed volume and surface area of the statue were 186,860 cm^3 and 24,670 cm^2, respectively. However, the measured volume and surface area calculated using the vision system were 179,387 cm^3 and 23,934 cm^2, respectively. Therefore, errors in the computed volume and surface area were 4% and 3%, respectively. These results indicate that the video measurement system is capable of competing with actual measurement procedures.

SUMMARY AND CONCLUSIONS

Integration of stereo vision technology and stereo photogrammetry algorithms described in this paper illustrates the usefulness of this approach in monitoring important historical sites. Using the minimum control requirements of measured distances and 3-D surveyed points on planar wall calibration facility gave the optimal, most accurate camera calibration model. The consistency of all tests, except those tests with 10 control distances and 20 control points, suggests that only the minimum control case need be used. The minimum control was found to be four surveyed 3-D control points located at the four corners of the planar wall and the measured distances between these points. This control array provides a practical, easy-to-use, effective, and accurate camera calibration procedure using a planar wall facility. Furthermore, the use of the planar wall calibration procedure in addition to the cubic calibration facility, with multiple model mapping, showed potential for accurate camera calibration as well as for convenient 3-D reconstruction of historical statues and monuments. This process could be extended to other applications of geometric measurements and other measurement tasks as well as to maintenance and restoration techniques.

Although the adapted stereo vision technique showed great potential for metrology applications, other problems in the adapted monitoring and mapping approach have yet to be investigated. Investigation of the method has to be extended to include the effects of the following factors on the planar wall calibration procedure: (1) waves and deviations; (2) camera warm-up; (3) image resolution; and (4) camera configuration—the base/object distance ratio.

APPENDIX I. REFERENCES

Abdel-Aziz, Y. I. (1982). "Accuracy of the normal case of close-range photogrammetry." *Photogrammetric Engrg. and Remote Sensing*, 48(2), 207–213.

Ahmed, F. A. (1981). "New simple photogrammetric techniques and their application in architecture and archeology." *Proc., 80s ERA of Change Fall Tech. Mtg.*, Honolulu, 424–430.

Epix, Inc. (1994). *Silicon video mux: User's manual, Version 6.8*. EPIX, Inc., Northbrook, Ill.

Fryer, J. G. (1989). "Camera calibration in non-topographic photogrammetry." *Non-Topographic Photogrammetry*, 2nd Ed., Am. Soc. for Photogrammetry and Remote Sensing, Falls Church, Va., 59–70.

Karara, H. M. (1989). *Non-Topographic Photogrammetry*, 2nd Ed., Am. Soc. of Photogrammetry and Remote Sensing, Falls Church, Va.

Ke, Y. (1995). "3-D body mapping with computer vision," PhD dissertation, Dept. of Civ. Engrg., Univ. of Illinois at Urbana-Champaign, Urbana, Ill.

Lew, M. S. (1990). "Hierarchical techniques in stereo matching," MS thesis, Dept. of Electrical Engrg., Univ. of Illinois at Urbana-Champaign, Urbana, Ill.

Obaidat, M. T., and Wong, K. W. (1996a). "Automated knowledge-based system for stereo video metrology." *J. Surv. Engrg.*, ASCE, 122(2), 47–64.

Obaidat, M. T., and Wong, K. W. (1996b). "Geometric calibration of CCD camera using planar object." *J. Surv. Engrg.*, ASCE, 122(3), 97–113.
Obaidat, M. T., Al-Suleiman, T. I., and Abdul-Jabbar, G. T. (1997). "Quantification of pavement rut depth using stereo vision technology." *J. Surv. Engrg.*, ASCE, 123(2), 55–70.
Pillmore, C. L., Coe, J. A., and Messerich, J. A. (1992). "Use of close-range photogrammetry to measure surface degradation of marble columns and capitals of the Merchants' Exchange, Philadelphia, Pennsylvania, U.S.A." *Proc., ASPRS/ACSM/RT '92 Convention: Mapping and Monitoring Global Change*, Vol. 2, Washington, D.C., 153–158.
Sherwood, S. I. (1992). "Stone decay in the context of pollution control: A status report on the first ten years of the American research program." *Proc., 7th Int. Congr. on Deterioration and Conservation of Stone*, Lisbon, Portugal.
Silva, L., and Gomes, C. (1992). "Using terrestrial photogrammetrics for maintenance of historical monuments." *Proc., ASPRS/ACSM/RT '92 Convention: Mapping and Monitoring Global Change*, Vol. 2, Washington, D.C., 142–152.
Wiley, A. G. (1991). "Metric aspects of zoom vision," PhD dissertation, Dept. of Civ. Engrg., Univ. of Illinois at Urbana-Champaign, Urbana, Ill.
Wiley, A. G., and Wong, K. W. (1992). "Geometric calibration of zoom lenses for computer vision metrology." *Int. Archives of Photogrammetry and Remote Sensing*, 29(5), 587–593.
Wong, K. W. (1980). "Basic mathematics of photogrammetry." *Manual of Photogrammetry*, 4th Ed., Am. Soc. of Photogrammetry, Fall Church, Va., 37–102.
Wong, K. W. (1992). "Machine vision, robot vision, computer vision, and close-range photogrammetry." *Photogrammetric Engrg. and Remote Sensing*, 58(8), 1197–1198.

APPENDIX II. NOTATION

The following symbols are used in this paper:

$\mathbf{A}$ = point where plane intersect x-axis;
$\dot{\mathbf{A}}$, $\ddot{\mathbf{A}}$ = residuals coefficient matrices for stereo image points and measured distances, respectively;
$\mathbf{B}$ = point where plane intersect y-axis;
$\dot{\mathbf{B}}$, $\ddot{\mathbf{B}}$ = coefficient matrices for stereo image points and measured distances, respectively;
C = point where plane intersect z-axis;
CCD = charge-coupled device;
DEM = digital elevation model;
f = camera focal length;
$\mathbf{I}$ = identity matrix;
k = affine scaling factor;
l_1, l_2 = radial distortion parameters;
m = number of stereo image points;
n = number of measured distances;
P_1, P_2, P_3 = decentering distortion parameters;
$\dot{\mathbf{V}}$, $\ddot{\mathbf{V}}$, $\ddot{\mathbf{V}}$ = residual matrices for stereo image points, measured distances, and unknown parameters, respectively;
X = x-axis coordinate of ground coordinate system;
X_i^c = x-axis coordinate of ground coordinate system for exposure center c of photo i;
x_{ij} = x-axis coordinate (in image domain) of image point j at photo i;

X_j = x-axis coordinate of ground coordinate system of ground point j;
x_p = x-coordinate of principal point;
Y = y-axis coordinate of ground coordinate system;
Y_i^c = y-axis coordinate of ground coordinate system for exposure center c of photo i;
y_{ij} = y-axis coordinate (in image domain) of image point j at photo i;
Y_j = y-axis coordinate of ground coordinate system of ground point j;
y_p = y-coordinate of principal point;
Z = z-axis coordinate of ground coordinate system;
Z_i^c = z-axis coordinate of ground coordinate system for exposure center c of photo i;
Z_j = z-axis coordinate of ground coordinate system of ground point j;
$\dot{\Delta}$ = vector of corrections for unknown parameters;
$\dot{\varepsilon}$, $\ddot{\varepsilon}$, $\ddot{\varepsilon}$ = discrepancy matrices for stereo image points, measured distances, and unknown parameters, respectively;
κ_r = rotation angle around z-axis of right image;
φ_r = rotation angle around y-axis of right image; and
ω_r = rotation angle around x-axis of right image.